Journal of Geoscience and Environment Protection, 2025, 13(2), 51-68
https://www.scirp.org/journal/gep
ISSN Online: 2327-4344
ISSN Print: 2327-4336

Efficient Identification Method of Interbeds Based on Neural Network Combined with Grey Relational Analysis

—Taking the Lower Sub-Member of the Sangonghe Formation in Moxizhuang Oilfield as an Example

Yuanbo Song[1,2], Yankai Zhu[1,2*], Binxin Zeng[1,2]

[1]School of Earth Science and Engineering, Xi'an Shiyou University, Xi'an, Shaanxi, China
[2]Shaanxi Provincial Key Laboratory of Petroleum Accumulation Geology, Xi'an, Shaanxi, China
Email: 976268446@qq.com, *1808113739@qq.com

How to cite this paper: Song, Y. B., Zhu, Y. K., & Zeng, B. X. (2025). Efficient Identification Method of Interbeds Based on Neural Network Combined with Grey Relational Analysis. *Journal of Geoscience and Environment Protection, 13,* 51-68.
https://doi.org/10.4236/gep.2025.132005

Received: January 6, 2025
Accepted: February 14, 2025
Published: February 17, 2025

Abstract

The storage layer within the Moxizhuang Oilfield in the Junggar Basin develops various types of interlayer barriers with significant differences in morphology and scale of development. In response to the issues of interlayer barriers affecting the formation of oil and gas reservoirs and controlling oil-water distribution, this study proposes precise classification and quantitative identification of interlayer barriers in the study area based on a fully connected neural network combined with grey relational analysis. Taking the second member of the Sangonghe Formation ($J_1S_2^2$) in the Moxizhuang Oilfield as an example, combined with previous research, this study statistically analyzes the lithology and logging response characteristics of three types of interlayer barriers in the study area. Based on differences in composition, lithology, and genesis, interlayer barrier types are classified. Sensitive logging data such as natural gamma, acoustic time difference, and resistivity are selected through crossover plots. Grey relational analysis is used to calculate comprehensive discrimination indicators for interlayer barriers. Combined with the fully connected neural network method, an interlayer barrier identification model is established, and model training is conducted to verify the accuracy of interlayer barrier identification. The results indicate that the interlayer barrier identification model based on a fully connected neural network can rapidly and accurately identify interlayer barriers and their types. Its application in the second member of the Sangonghe Formation in the Moxizhuang Oilfield in the Junggar Basin has proven that the identification results of this method for interlayer barriers have a conformity rate exceeding 90% with core data, demonstrating excellent

performance in interlayer barrier identification and proving the effectiveness of the model for interlayer barrier identification and prediction in this area. The research conclusions can provide theoretical guidance and technical reference for the identification and evaluation of interlayer barriers in the second member of the Sangonghe Formation in the Moxizhuang Oilfield in the Junggar Basin.

Keywords

Interlayer Recognition, Grey Relational Analysis, Fully Connected Neural Network, Second Member of Sangonghe Formation

1. Introduction

The term "interlayer" refers to the impermeable or low-permeability layers that are interspersed within the reservoir and have significant differences in physical properties from the reservoir. These layers can hinder or isolate the flow of fluids within the layer, affecting the development and production processes of oil field (Jiang et al., 2014). The thickness of interlayers is usually from tens of centimeters to several meters, which cannot effectively block or regulate the flow of fluids, but it can affect the local oil layers in the vicinity, to varying degrees, limiting the movement of reservoir fluids and making it easier to form relatively independent oil-water systems between layers, which greatly affects the flow patterns of oil and gas within the reservoir. The qualitative identification of interlayers is mostly based on core-log analysis, and commonly uses traditional core observation methods, data cross-plotting methods, and geological statistics (Li et al., 2020; Yang et al., 2014; Zhou et al., 2017). The identification accuracy for small-scale and discontinuous interlayers within the reservoir is relatively low. In recent years, with the rapid development of artificial intelligence technology in oil and gas exploration, development, and production (Huang et al., 2023), interdisciplinary technical methods combined with machine learning algorithms have been widely applied in the study of interlayers. Qu Ziyi et al. (Qu et al., 2009) proposed using wavelet neural networks to establish recognition models for log response parameters that reflect interlayers in carbonate reservoirs, Chen Wei et al. (Chen et al., 2011) proposed building neural network interpretation models for log curves and pore permeability to standardly discriminate interlayers, Chen Xiu et al. (Chen et al., 2021) proposed using support vector machine classification capabilities and principal component analysis dimensionality reduction techniques to identify interlayers in braided river reservoirs, and Si Yang et al. (Si et al., 2023) proposed using self-organizing neural networks and K-nearest neighbor algorithms for quantitative identification of interlayers, Jiao Shixiang et al. (Jiao et al., 2023) proposed an improved model based on autoencoders for the identification of interbedded layers. These methods have all shown significant improvements in accuracy in the process of identifying interlayers.

The Mosizhuang oil field is characterized by a low oil saturation reservoir, and the San Gonghe Formation, serving as the main oil-bearing stratum, is confronted with development challenges such as limited remaining recoverable reserves and the intricate distribution of residual oil. Moreover, the Mosizhuang region is marked by a pattern of multi-sand body superimposition and contiguous distribution, with individual sand bodies capable of forming independent oil reservoirs. The degree and distribution of interlayer development within the reservoir further complicate the oil-water relationships. Consequently, precise identification of interlayers is crucial for understanding their impact on the distribution of oil and water, and it is one of the key elements in enhancing the recovery rate of the reservoir (Deng et al., 2016; Yin et al., 2013) The study focuses on the lower submember of the second member of the San Gonghe Formation ($J1s2^2$) in the Mosizhuang oil field, utilizing core, logging, well logging, and development dynamic data. It selects logging curves sensitive to interlayers and establishes a quantitative identification template for interlayers by integrating comprehensive discriminative indicators with fully connected neural networks. Additionally, it analyzes the influence of interlayers on the distribution of oil and water, with the goal of improving the precision and efficiency of interlayer identification and delineation in the study area, as well as contributing to the potential exploration and enhancement of reservoir efficiency.

2. Overview of the Study Area

The Moxizhuang area is located in the hinterland of the Junggar Basin, situated on the southwestern fringes of the Gurbantunggut Desert in the central part of the Junggar Basin. It is mainly distributed in the central uplift zone of the Junggar Basin and structurally situated in the transitional slope zone between the Mosuowan uplift of the central depression of the Junggar Basin and the western depression of Well Ban-1 (Meng, 2020) (as shown in **Figure 1**). It also exhibits a northeast-southwest trending nose-like structure (Bi et al., 2011). The target formation in the Moxizhuang oilfield area is the Jurassic Sangonghe Formation, with a stratigraphic thickness of 300 to 400 meters. From bottom to top, it is divided into J1S3, J1S2, and J1S1. J1S2 serves as the main oil-producing layer of the Moxizhuang reservoir, with a stably developed frontal mud (mud neck) of about 10 to 30 meters thick in the middle. With the mud neck as the boundary, it can be divided into two sub-intervals: the upper member of the Sangonghe Formation ($J1S2^1$) and the lower member of the Sangonghe Formation ($J1S2^2$) (Cheng, 2023). Among them, the second member of the Sangonghe Formation ($J1S2^2$) is the main oil-bearing interval, with a sedimentary facies of braided river delta front subfacies. The reservoir sandstone bodies are widely distributed and have a relatively stable thickness, reaching 60 to 100 meters. The oil layers are concentrated in the upper part of $J1S2^2$, where the spatial distribution of interbedded shales and barriers is complex, and the heterogeneity is strong, characterized by medium-to-low porosity and low permeability reservoirs (Zhang et al., 2014).

Figure 1. Location of the study area.

3. Characteristics of Interbedded Shales and Barriers

The second member of the Sangonghe Formation ($J_1S_2^2$) in the Moxizhuang area develops relatively stable sandstone deposits. Due to strong hydrodynamic conditions and frequent erosion, fewer fine facies belts can be observed in the cores, indicating that the deposition may have occurred in an area with multiple channel developments. This depositional characteristic results in the well-developed interbedded shales and barriers within the $J_1S_2^2$ sandstone bodies. Based on the lithological characteristics and genetic mechanisms of the interbedded shales and barriers, they can be classified into mudstone interbeds, fine sandstone physical property barriers, and calcareous sandstone interbeds in the study area, according to lithological differences and genesis (Deng, 2016).

3.1. Types of Interbedded Shales and Barriers and Their Logging Response Characteristics

Mudstone interbeds are composed of layers with high mud content, such as gray mudstone, silty mudstone, and light gray muddy fine sandstone. These interbeds typically have low permeability and strong sealing ability, and they are widely and stably developed in $J_1S_2^2$ with a certain degree of continuity. The distribution and scale of most mudstone interbeds are closely related to sedimentary microfacies (Deng, 2016), and they are mostly developed in sedimentary microfacies such as frontal mud, underwater natural levees, interdistributary bays, and distal bars. Due to the high mud content of mudstone interbeds, their logging curve response characteristics are similar to those of mudstone, with the most notable manifestation being a high natural gamma value, and the curve showing medium-to-high amplitude tongue-shaped or high-amplitude finger-shaped protrusions; the spontaneous potential amplitude decreases without obvious anomalies, and the curve

is close to the mudstone baseline; the resistivity index is relatively low, with little or no difference in the amplitude between deep and shallow induction resistivity; the density value is low, and the curve appears as a low-amplitude tongue shape; both acoustic time difference and compensated neutron values are relatively high.

Physical property barriers composed of fine sandstone mainly develop in low-permeability intervals within the formation, with lithologies mainly being light gray massive fine sandstone and siltstone containing multiple fine-grained materials and poor sorting. Although these barriers are mainly low-permeability, they still have a certain degree of permeability and porosity, but their physical properties are relatively poor. The logging curve response characteristics of physical property barriers composed of fine sandstone fall between those of mudstone and calcareous interbeds, with the natural gamma being moderate and the curve showing medium-amplitude protrusions; the spontaneous potential exhibits a decrease in negative anomaly amplitude; the density value is low but higher than that of mudstone interbeds; the wellbore diameter curve shows no significant expansion; the spontaneous potential curve shows a reversal or slight reversal phenomenon.

Calcareous sandstone interbeds mainly develop in sandstone intervals with better internal physical properties. Under the control of secondary diagenesis, strong calcitic cementation within the sandstone intervals clogging pores, resulting in extremely poor porosity development. At the same time, the development degree of these interbeds in the area is poor, and their distribution is relatively random. The most significant logging curve response characteristic of calcareous interbeds is that the deep and shallow resistivity show abnormally high values, with the curve appearing as sharp peak finger shapes; the wellbore diameter curve does not change significantly; due to pore cementation by calcium, the acoustic time difference shows abnormally low values, but the density is high, generally greater than 2.2 g/cm^3 (as shown in **Figures 2(a)-(c)**).

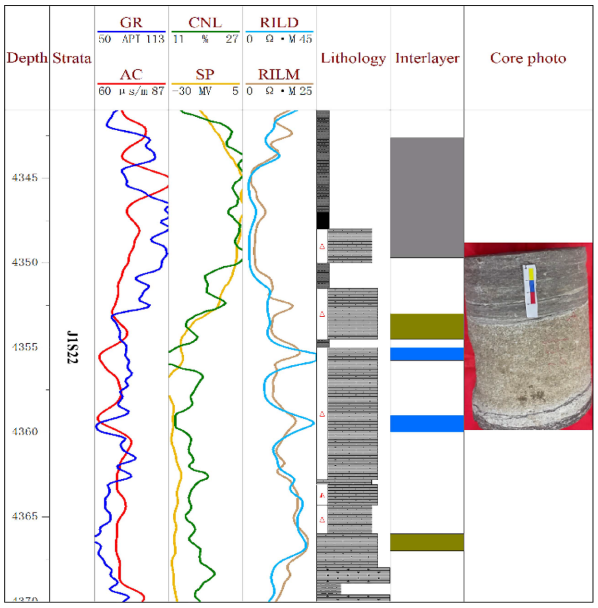

(a) Argillaceous rock interlayer 1

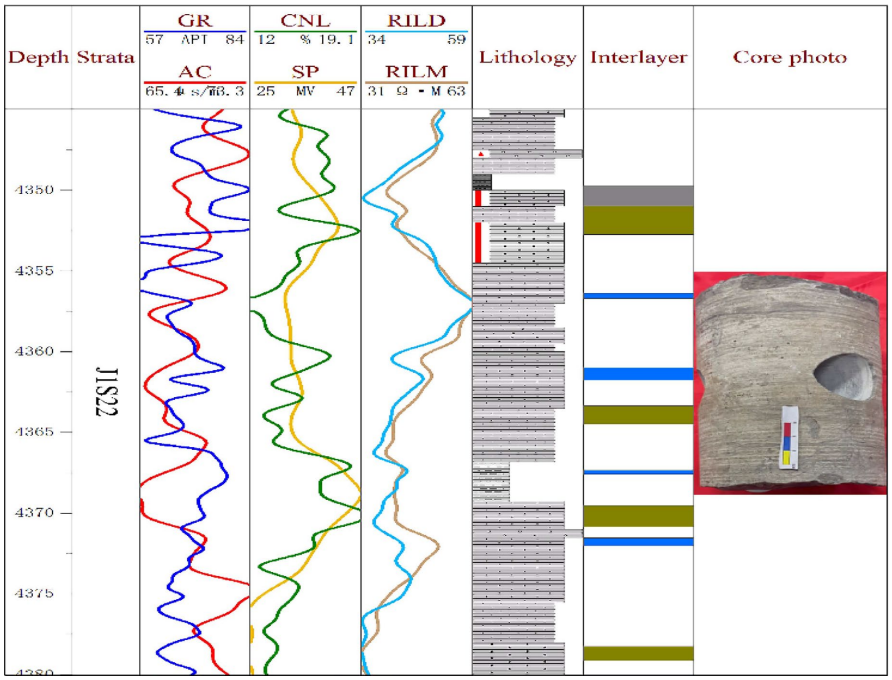

(b) Physical property interlayer

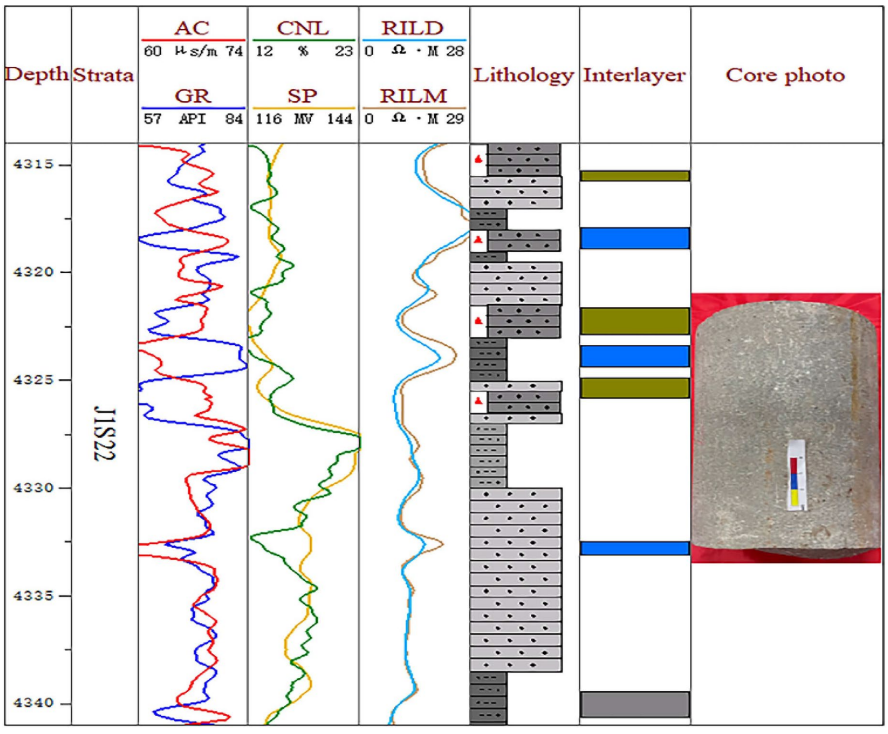

(c) Calcareous interlayer

Figure 2. Lithology, logging responses, and core characteristics of different types of interbeds and barrier layers.

3.2. Selection of Sensitive Logging Parameters for Interbedded Shales and Barriers

Using cross-plot technology, we analyzed the response characteristics of various

logging curves, including natural gamma (GR), deep induction resistivity (RILD), density (DEN), spontaneous potential (SP), acoustic time difference (AC), and compensated neutron logging (CNL). These analyses were calibrated with core data (Yi et al., 2021). It was found that different types of interbedded shales and barriers exhibited strong responses to logging curves, such as natural gamma, acoustic time difference, resistivity, and density (**Figure 3**). As shown in the figure, muddy interbedded shales are characterized by high acoustic time difference, high natural gamma, and low resistivity in logging responses, while calcareous interbedded shales show low acoustic time difference, low natural gamma, and high resistivity. The physical property interbedded shales fall between these two types. Finally, eliminate parameters that are correlated. Choose either the sonic transit time or the density curve to be included in the selection of natural gamma, deep induction resistivity, sonic transit time, and permeability as the sensitive logging parameters for identifying interbed types. Establish a logging response sample set for each lithological interbed.

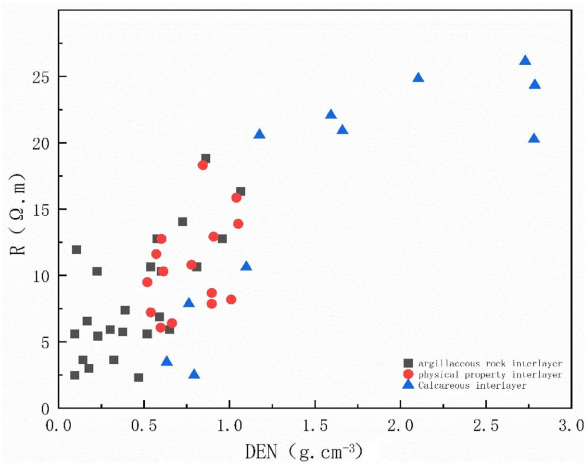

(a)

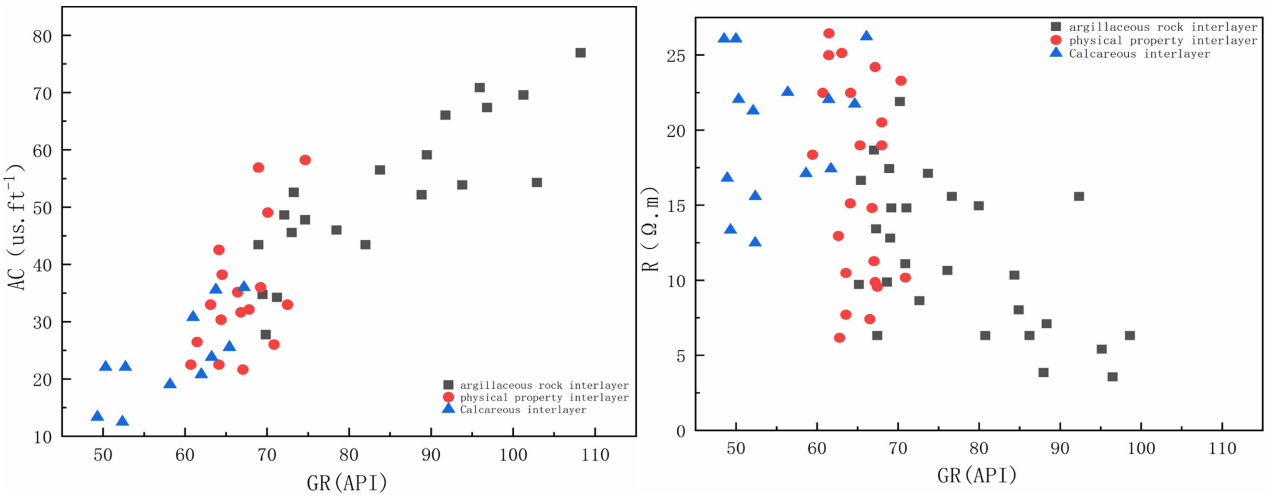

(b) (c)

Figure 3. Logging cross-plots for identifying interbeds and barrier layers.

4. Neural Network Discrimination of Interbedded Shales and Barriers

4.1. Algorithm Introduction

4.1.1. Full Connected Neural Network (FCNN)

The Full Connected Neural Network (FCNN) is a neural network based on the single-layer perceptron network, which introduces multiple hidden layers to enhance its ability to learn and capture complex data features (Karande & Kalbande, 2018). Theoretically, the FCNN possesses powerful function approximation capabilities, meaning it can theoretically fit any function, with a particularly strong ability to fit nonlinear functions. As the number of hidden layers increases, the expressive power of the neural network also strengthens (Jin et al., 2024). It can recognize the feature relationships between input data and labels, thereby enabling complex information processing and reasoning functions. Through learning, the neural network can continuously optimize its performance and accuracy (Bai et al., 2024). The basic structure of the FCNN includes an input layer, hidden layers, and an output layer. Each layer is interconnected by several neurons, with no neuron connections within the same layer. The input layer is mapped to the output layer through simple arithmetic operations represented by neurons (Zhong et al., 2024) (**Figure 4**). The basic structure of the FCNN is as follows:

1) Input Layer: Relevant feature vectors from the training sample data are input. The number of feature vectors determines the number of input nodes, and no function processing is performed at this layer.

2) Hidden Layers: The hidden layers are the core of the FCNN. The number of hidden layers and the number of neurons in each layer are adjusted according to specific tasks. These layers perform nonlinear transformations and feature extraction on the training sample data. Subsequently, feature information is exchanged between neurons and passed to the activation function for processing. After processing, the new feature information is transmitted to the next layer. To effectively prevent overfitting of the model, this paper adopts the Rectified Linear Unit (ReLU) activation function, which is defined as follows:

$$\mathrm{ReLU}(x) = \max(0, x) \tag{1}$$

The calculation formula for the hidden layer is:

$$y = R\left(W^l t + b^l\right) \tag{2}$$

In the formula: y represents the output value of the hidden layer; t represents the input value of the hidden layer; W^l denotes the weights of the L-th hidden layer; b^l represents the bias vector of the L-th hidden layer; R stands for the ReLU function.

3) Output Layer: This layer is the last layer of the neural network, responsible for converting the learned features or patterns into final prediction results or classification labels.

4.1.2. Grey Relation Analysis

Grey Relation Analysis (GRA) is employed to calculate comprehensive discriminant

indicators. This technique is primarily used to quantify the grey relational degree among various parameters. This method is often applied to analyze the degree of association between different factors or indicators (Lee et al., 2012). In grey systems, due to incomplete or uncertain information, GRA provides a way to quantify these degrees of association. The application of this analysis method to the study of interbeds essentially involves a comprehensive evaluation of multiple parameters. The core essence lies in determining the weight coefficients of multiple parameters for interbeds, ultimately obtaining a comprehensive discriminant indicator, and relying on it to classify interbeds.

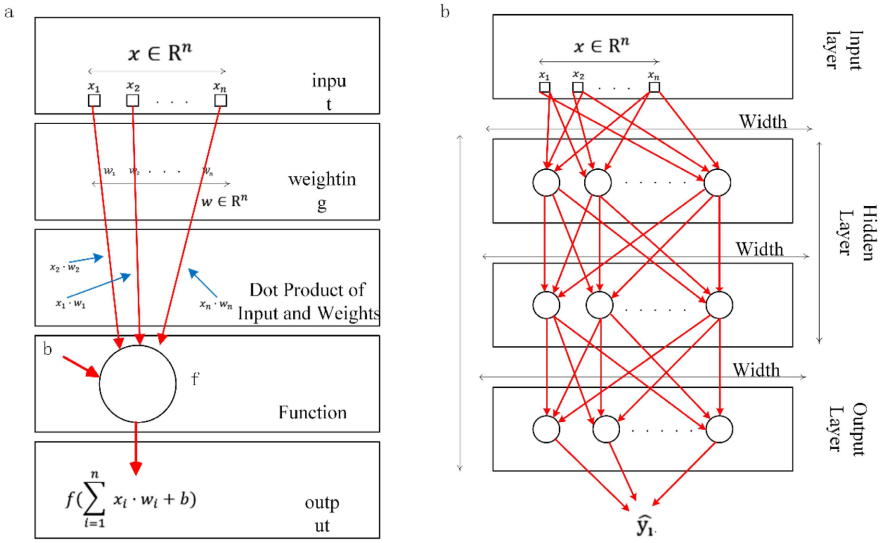

Figure 4. The topological structure of a neural network. (a) Internal function computation; (b) External architecture. $x=(x_1,x_2,\cdots,x_n)^{\mathrm{T}}$, represents the attribute vector; $w=(w_1,w_2,\cdots,w_n)^{\mathrm{T}}$, represents the weight vector; b denotes the bias coefficient; f represents the activation function; $\hat{y}_i$ represents the output value. Quoted from literature (He et al., 2023).

4.2. Interbed Identification and Analysis Process

The current identification and analysis are primarily conducted on the basis of preprocessed research data, including routine core analysis, well logging data normalization, and relevant geological information. Firstly, a comprehensive discriminant indicator for interbeds is calculated. Subsequently, a Fully Connected Neural Network (FNCC) is used to learn from this comprehensive discriminant indicator, enhancing the ability of multi-well logging data to characterize differences in responses to various interbeds. Meanwhile, an interbed identification network model is constructed. The specific process is illustrated in **Figure 5**. The well logging data from the Moxizhuang Oilfield in the study area is complex, with missing and abnormal values. Additionally, the nature of the well logging data results in inconsistent units and orders of magnitude. Therefore, preprocessing of the well logging data is carried out, including normalization, which can be

expressed by the formula:

$$Y = \frac{X - X_{\min}}{X_{\max} - X_{\min}} \tag{3}$$

In the formula: Y represents the normalized structure; X represents the original well logging data; $X_{\max}$ and $X_{\min}$ represents the maximum and minimum values of the original well logging data, respectively.

1) Comprehensive discriminant indicator: Natural gamma, acoustic time difference, and resistivity are selected as the sensitive parameters for well logging. The grey relational degree theory is employed for calculation. The calculation formula and process are shown in **Figure 6**. Firstly, the original data is dimensionless through averaging. Then, the grey relational coefficient of each data is calculated, followed by the calculation of the relational degree of each parameter (Yi et al. 2021). Ultimately, the weight coefficients of natural gamma, deep lateral resistivity, and acoustic time difference for identifying interbeds in the Moxizhuang j2S2 formation are determined to be 0.32, 0.34, and 0.3, respectively. When the discriminant parameters and their weight coefficients for interbeds are obtained, the obtained weight parameters are multiplied by the sensitive parameters to calculate the comprehensive discriminant indicator for interbeds (I-interlayer = 0.32 × GR + 0.34 × RILD + 0.3 × AC) for qualitative identification of interbeds. By calibrating the calculated I-interlayer value of the cored wells with the core samples from the cored intervals, the comprehensive discriminant indicators for the target layer can be classified, with I-interlayer ≥ 60 indicating a shale interbed, 55 ≤ I-interlayer ≤ 60 indicating a calcareous interbed, and I-interlayer ≤ 55 indicating a physical property interbed.

2) Construction of a full neural network: The comprehensive discriminant indicators for interbeds from four wells (Z1, Z101, Z103, Z107) in the study area are selected for training and divided into a training set and a validation set in a ratio of 8:2. Additionally, the comprehensive discriminant indicators for interbeds from two other wells (Z109, Z110) are selected as a test set. Subsequently, the training set and validation set are used to train the fully connected neural network model. To achieve optimal results for the neural network model, the mean squared error loss function (Equation 3) is employed during forward propagation to calculate the distance between the true value and the predicted output value, thereby obtaining the error of the current model. The gradient descent method (Hochreiter et al., 2001) is used for training the backpropagation of errors to gradually adjust and update the network weights and bias parameters between layers, thereby optimizing the parameters of the neural network model. After multiple iterations, the convergence of the loss function is observed, as shown in **Figure 7(a)**, where the loss function is small and convergent. At this point, the optimal fully connected neural network prediction model is constructed. After construction, the validation set is input into the model for recognition, analysis, and processing to assess whether the neural network model meets the expected accuracy requirements, as shown in **Figure 7(b)**. Once the recognition accuracy requirements

are met, an interbed identification network model is obtained. Finally, the test set is used to verify the recognition effect, achieving the effect of interbed identification, as shown in Figure 7(c).

$$MSE = \frac{1}{n}\sum_{i=1}^{n}\left(y_i' - y_i\right)^2 \tag{4}$$

In the formula: y_i represents the true value of the i-th sample; y_i' represents the predicted value of thei-th sample; n represents the number of samples.

Figure 5. Identification process of interbeds and barrier layers based on Fully Connected Neural Network (FCNN).

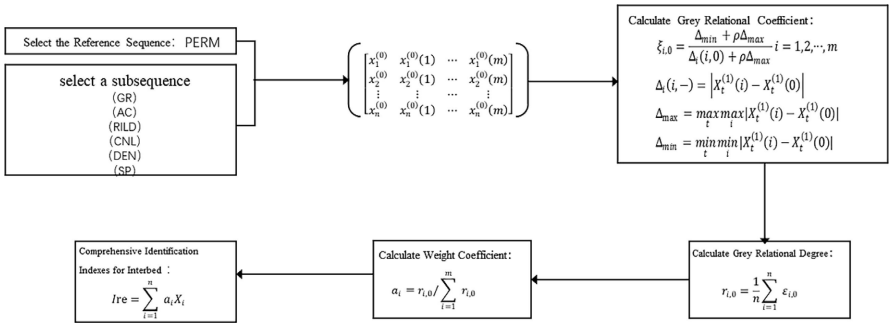

Figure 6. Calculation process of comprehensive discriminant indicators.

4.3. Identification Effectiveness

The identification of interbeds in some wells in the study area was validated using core data, classification criteria for interbed identification, and reservoir intervals interpreted from well logging results. Meanwhile, conduct a performance comparison of similar algorithms, and use the K-means and KNN algorithms to train and test the data samples respectively. 1) K-means algorithm for interbed division: With k = 3 as the clustering center, the training accuracy of the interbed division using this algorithm reaches 94.5%, and the prediction accuracy for the test data reaches 92.1%. 2) KNN algorithm for interbed division: With k = 8 and using Euclidean distance, the KNN algorithm is applied to train the interbed sample data, achieving a training accuracy of 93.7%, and the prediction accuracy for the test data is 91.5%. The use of K-means and KNN algorithms for interbed division in the study area shows that both the training and testing accuracies are lower than those of the GRA-FCNN algorithm, proving that the GRA-FCNN algorithm performs better in the study area. A comprehensive evaluation of the effectiveness of interbed identification and classification was conducted on the vertical plane of individual wells (**Figure 8**). Through comparative analysis of core data and well logging identification results, the coincidence rate for identifying the types and quantities of interbeds exceeded 90%. According to the identification statistics, the thickness of shale-type interbeds in the second member of the Sangonghe Formation ($J_1S_2^2$) in the study area ranged from 4.4 to 19.6 meters, with a distribution frequency of 0.016 to 0.129 layers per meter. These shale-type interbeds are widely and stably developed at the top and within $J_1S_2^2$ (**Table 1**). The development of fine-grained sandstone physical property interbeds and calcareous sandstone interbeds is generally poor, with similar distribution frequencies and densities. Both types belong to intra-layer interbeds and their development varies in different well areas. The sealing and permeability capabilities of these two types of interbeds are much lower than those of shale interbeds. Their higher distribution frequencies and densities within the reservoir will greatly restrict fluid migration and accumulation.

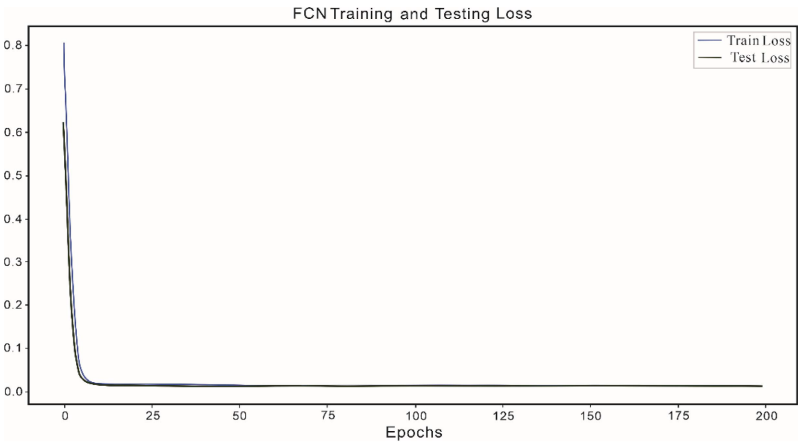

(a) The convergence of the model's loss function

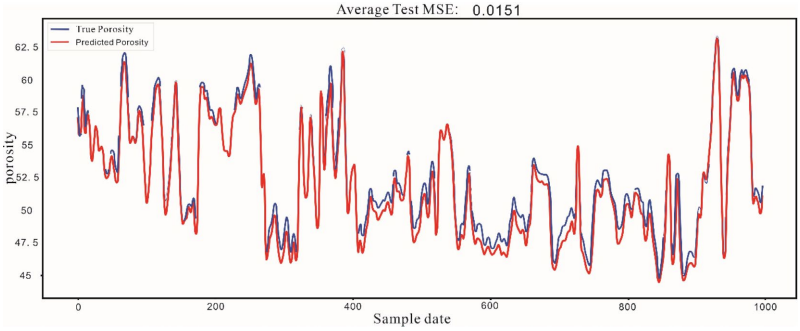

(b) Model training and prediction performance

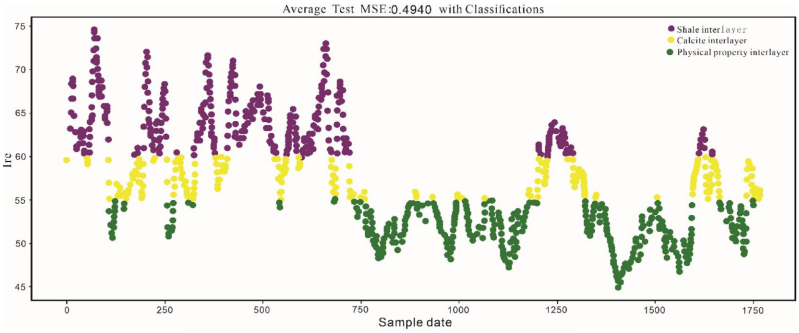

(c) Model prediction classification performance

Figure 7. Training and learning of neural network models, as well as their classification and prediction effectiveness.

Table 1. Distribution of different interlayer spacers.

types of intercalated layers	distribution frequency (layer/m)	average distribution frequency	distribution density	average distribution density
clay interbedded layers	0.016 - 0.129	0.055	0.063 - 0.237	0.112
fine-grained sandstone interlayer with distinct physical characteristics	0.026 - 0.098	0.059	0.034 - 0.186	0.089
calcareous sandstone interlayer	0.026 - 0.067	0.044	0.029 - 0.091	0.07

4.4. Analysis and Discussion

Traditional methods for identifying and classifying interbeds often face issues of insufficient accuracy and low efficiency. To address this problem, a quantitative identification method based on a fully connected neural network combined with grey relational analysis is proposed. This method has demonstrated a high degree of effectiveness in practical applications, but there are still some key issues to be addressed and resolved. For neural networks, feature learning is often used for prediction and classification labeling. Since its fully connected neural network cannot automatically extract features, it usually relies on manually designed features or specific data preprocessing steps for feature extraction. Insufficient data quantity and the presence of erroneous or misleading learning features in the actual data will inevitably introduce some errors. Although data normalization is

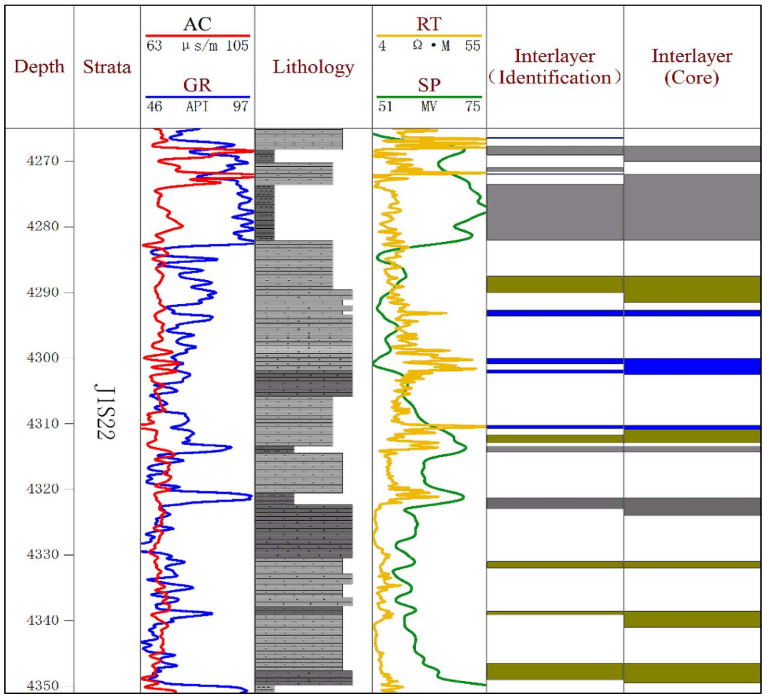

Figure 8. Actual verification effect of a single well.

performed, errors will still exist. For example, the logging environment of each well leads to differences in logging data quality, and the heterogeneity of reservoir geological characteristics, such as wellbore conditions affecting GR and other radioactive logging methods, different resistivity logging methods affecting RILD and other resistivity logging curves, and formation water salinity affecting SP curve amplitudes (Si et al., 2023). Therefore, when applying this method to different regions and reservoirs with varying degrees of heterogeneity, besides standardizing the necessary logging curve data, corresponding adjustments and corrections can also be made to the logging environment and sensitive logging parameters.

From the results, the overall identification effect for thicker shale-type interbeds is good, with errors mainly distributed in the identification of thin interbeds, such as physical property interbeds and calcareous sandstone interbeds. This method can still identify and classify thin interbeds within sand bodies that were not previously classified by original logging interpretations or were not obviously observed in cores, and the identified and classified interbeds within the reservoir are more detailed, which is the main reason for the identification errors in thin interbeds.

5. Impact of Interbeds on Oil-Water Systems

In early understandings of the study area, the Sangonghe Formation did not develop faults internally and was mainly controlled by lithological traps for hydrocarbon accumulations (Xie et al., 2004). In recent years, with advancements in drilling technology and the accumulation of seismic data, the existence of small

faults and interlayer faults in this area has gradually been recognized. Although these faults cannot effectively block oil and water, the widespread development of interbeds, combined with these faults, produces a sealing effect on the reservoir and thus influences the oil-water system. Under this influence, interbeds have two controlling effects on the reservoir:

On the one hand, interbeds form multiple independent reservoirs through vertical and lateral shielding. Different types of interbeds exhibit complexly interwoven and superimposed distribution characteristics in space, effectively dividing the internal space into many relatively independent fluid units. During hydrocarbon migration, the abundant interbeds developed within the reservoir form vertical shielding, causing lateral migration, and oil, gas, and water enter these units to form multiple independent reservoirs (Deng, 2016). At the same time, well-connected and widely developed shale-type interbeds provide upper shielding for oil, gas, and water, making it difficult for them to migrate through these areas, thus forming a sealing layer that prevents upward migration of oil, gas, and water. On the other hand, lateral sealing by interbeds can lead to changes in the oil-water system, small-scale faults developed in the study area create a special spatial configuration relationship between the faults and reservoir sand bodies. This relationship causes continuous sand bodies to be faulted, resulting in differences in lithology on both sides of the fault. The originally connected horizons with the sand bodies become interbeds or sealing layers, so that interbeds control the distribution of oil, gas, and water vertically and laterally, and can also play a role in lateral sealing even when the reservoir closure height is not large (Wang et al., 2006).

6. Conclusion

1) By effectively screening the conventional well logging curves of the Sangonghe Formation in the Moxizhuang Oilfield, more sensitive curve parameters for identifying the interbeds and barriers were selected. Subsequently, grey relational analysis was used to calculate comprehensive discriminant indicators for the interbeds and barriers. When combined with a fully connected neural network model, it could better identify the interbeds and barriers as well as their types. Moreover, this method has lower requirements for the number of data samples and can also produce corresponding prediction results after processing small samples without typical distribution patterns. Therefore, it has practical application value and broad application and development prospects in identifying interbeds and barriers during production.

2) After accurately identifying the interbeds and barriers, from the perspective of their distribution in individual wells and the interpretation of connected well profiles, it can be observed that vertically, the number of interbeds and barriers developed within each well varies, and their distribution is uncertain. These interbeds and barriers divide the complete fluid units of the reservoir into relatively independent fluid units. Horizontally, muddy rock interbeds and barriers exhibit continuity, while the other two types have poor continuity and correlation

between wells. It can be inferred that interbeds and barriers typically develop only locally and have a significant impact on local oil and water distribution.

3) The formation of the Sangonghe Formation in the Moxizhuang Oilfield has undergone changes in depositional environments and later diagenesis, resulting in the widespread development of numerous interbeds and barriers within the formation. Additionally, numerous small-scale compressive-torsional faults have developed in the area, causing dislocations in the originally continuous sand layers and resulting in differences in lithology on both sides of the faults. Consequently, the interbeds and barriers not only achieve effective vertical sealing but also provide lateral sealing capabilities. Therefore, under the dual effects of faults and interbeds, the originally unified oil-water system in the area has been divided into relatively independent oil-water systems in most well areas.

Chengdu University of Technology; Exploration and Development Research Institute, Qinghai Oilfield Company, China National Petroleum Corporation; 8.

Zhao Dongsheng., Zhang Min., Zhang Daowei., et al. (2015). Maturity of Oil Source in the Paleogene and Neogene of Western Qaidam Basin. *Acta Sedimentologica Sinica,* 2007, (02): 319-324. (Note: The year "2007" in the bracket seems to be a mistake b.

Conflicts of Interest

The authors declare no conflicts of interest regarding the publication of this paper.

References

Bai, W., Cheng, S., Guo, X., Wang, Y., Guo, Q., & Tan, C. (2024). Oilfield Analogy and Productivity Prediction Based on Machine Learning: Field Cases in PL Oilfield, China. *Petroleum Science, 21,* 2554-2570. https://doi.org/10.1016/j.petsci.2024.02.018

Bi, Y., Gao, S., & Zhu, Y. (2011). Hydrocarbon Accumulation Patterns of Moxizhuang Oilfield, the Junggar Basin. *Oil & Gas Geology, 32,* 318-326.

Chen, W., He, J., & Yang, B. (2011). Study on Logging Identification of Interbeds and Barriers in DH Oilfield. *Computing Techniques for Geochemical and Calculation Techniques, 33,* 202-205.

Chen, X., Xu, S., & Li, S. (2021). Identification of Interlayers in Braided River Reservoir Based on Support Vector Machine and Principal Component Analysis. *Journal of China University of Petroleum (Edition of Natural Science), 45,* 22-31.

Cheng, K. (2023). *Characteristics and Genesis of Low Oil Saturation Reservoirs in the Moxizhuang Oilfield of the Junggar Basin*. Xi'an Shiyou University.

Deng, X. (2016). Characteristics of Heterogeneous Interbeds in the J_1s_2 Reservoir of Block 1 in the Central Junggar Basin. *Science Technology and Engineering, 16,* 27-31.

Deng, Y., Guo, R., Tian, Z., Tan, W., Yi, Y., Xu, Z. et al. (2016). Geologic Features and Genesis of the Barriers and Intercalations in Carbonates: A Case Study of the Cretaceous Mishrif Formation, West Qurna Oil Field, Iraq. *Petroleum Exploration and Development, 43,* 136-144. https://doi.org/10.1016/s1876-3804(16)30018-0

He, T., Zhou, N., & Wu, X. (2023). Prediction of Effective Sandstone Thickness in Reservoirs Based on Deep Fully Connected Neural Networks. *Journal of Jilin University (Earth Science Edition), 53,* 1262-1274.

Hochreiter, S., Younger, A. S., & Conwell, P. R. (2001). Learning to Learn Using Gradient Descent. In G. Dorffner, H. Bischof, & K. Hornik (Eds.), *Lecture Notes in Computer Science* (pp. 87-94). Springer. https://doi.org/10.1007/3-540-44668-0_13

Huang, Y., Li, X., Liu, X., Zhai, Y., Fang, F., Guo, W. et al. (2023). Review of the Productivity Evaluation Methods for Shale Gas Wells. *Journal of Petroleum Exploration and Production Technology, 14,* 25-39. https://doi.org/10.1007/s13202-023-01698-z

Jiang, P., Huang, J., Lei, X., Cheng, C., & Zhang, Y. (2014). Study on Interlayer Distribution of I Oil Group in Member 2 of Zhujiang Formation in a Oilfield. *Journal of Southwest Petroleum University, 36,* 19-26.

Jiao, S., Zhao, J., He, Y., Zhao, S., Wu, Z., Zeng, T. et al. (2023). Semi-Supervised Interlayer Intelligent Recognition Method. *Earth Science Informatics, 16,* 2187-2197. https://doi.org/10.1007/s12145-023-01021-8

Jin, Y., Guo, K., Gao, X., & Li, Q. (2024). Tight Oil Well Productivity Prediction Model Based on Neural Network. *Processes, 12,* Article No. 2088. https://doi.org/10.3390/pr12102088

Karande, A. M., & Kalbande, D. R. (2018). Weight Assignment Algorithms for Designing Fully Connected Neural Network. *International Journal of Intelligent Systems and Applications, 10,* 68-76. https://doi.org/10.5815/ijisa.2018.06.08

Lee, P. T., Lin, C., & Shin, S. (2012). A Comparative Study on Financial Positions of Shipping Companies in Taiwan Region and Korea Using Entropy and Grey Relation Analysis. *Expert Systems with Applications, 39,* 5649-5657. https://doi.org/10.1016/j.eswa.2011.11.052

LI, F.-F., Guo, R., & Liu, L.-F. (2020). Identification of Interlayer in Thick Carbonate Reservoir under the Control of Genesis. *Science Technology and Engineering, 20,* 3650-3657.

Meng, L. (2020). Lower Limits of Physical Properties of Sandstone Reservoirs in the Second Member of Sangonghe Formation in Moxizhuang Oilfield. *Xinjiang Petroleum Geology, 40,* 557-564.

Qu, Z., Luo, X., & Xie, R. (2009). Application of Wavelet Neural Network in the Study of Interlayer. *Journal of Oil and Gas Technology, 31,* 265-268.

Si, Y., Cai, M. J., & Zhang, J.L. (2023). Quantitative Identification Method of Reservoir Flow Barriers Based on Self-Organizing Neural Network and K-Nearest Neighbor Algorithm. *Journal of China University of Petroleum (Edition of Natural Science), 47,* 35-47.

Wang, Y., Lin, C., & Wen, C. (2006). Analysis of the Control Effect of Interlayers on Oil Reservoirs: A Case Study of the Sangonghe Formation in the Moxizhuang Area of Block 1 in the Central Junggar Basin. *Petroleum Geology and Recovery Efficiency, 13,* 17-20.

Xie, X., Deng, H., & Wang, J. (2004). Integration of Seismic Processing and Interpretation for Fine Reservoir Characterization: Taking Moxizhuang Area in Junggar Basin as an Example. *Oil & Gas Geology, 25,* 533-538.

Yang, F., Liao, M., & Wang, Q. (2014). The Use of Logging Data in Identifying the Interlayer in Tazhong Oilfield 4. *Chinese Journal of Engineering Geophysics, 11,* 487-492.

Yi, S., Wang, L., & Ni, J. E. (2021). Characteristics and Geological Significance of Mixed Reservoir Interbeds in the Asmari Formation of the M Oilfield in Iraq. *Journal of Xi'an University of Science and Technology, 41,* 1014-1024.

Yin, S., Wu, S., & Feng, W. (2013). Patterns of Inter-Layers in the Alluvial Fan Reservoirs: A Case Study on Triassic Lower Karamay Formation, Yizhong Area, Karamay Oilfield, NW China. *Petroleum Exploration and Development, 40,* 757-763.

Zhang, J., Liu, C., & Zhu, G. (2014). Characteristics and Genesis of Low-Permeability

Reservoirs in the Moxizhuang Oilfield. *Special Oil and Gas Reservoirs, 21,* 58-61.

Zhong, Z., Ni, B., & Shi, Y. (2024). Response Analysis of Subway Stations and Optimization of Seismic Intensity Indices Based on Fully Connected Neural Networks. *Chinese Journal of Geotechnical Engineering, 46,* 567-577.

Zhou, X., Ding, W., & Chang, L. (2017). Three End-Member Diagram of Classification to Identify the Interlayers of Sandstone Reservoir in Littoral Facies: A Case from Carboniferous Donghe Sandstone in Hade Oil Field, Tarim Basin, NW China. *Earth Science Frontiers, 24,* 328-338.